

Internal structure of the San Andreas fault at Parkfield, California

Martyn J. Unsworth

Geophysics Program, University of Washington, Seattle, Washington 98195

Peter E. Malin

Department of Geology, Duke University, Durham, North Carolina 27708

Gary D. Egbert

College of Oceanic and Atmospheric Sciences, Oregon State University, Corvallis, Oregon 97331

John R. Booker

Geophysics Program, University of Washington, Seattle, Washington 98195

ABSTRACT

Magnetotelluric and seismic reflection surveys at Parkfield, California, show that the San Andreas fault zone is characterized by a vertical zone of low electrical resistivity. This zone is ≈ 500 m wide and extends to a depth of ≈ 4000 m. The low electrical resistivity is attributed to high porosity of saline fluids present in the highly fractured fault zone. The occurrence of microearthquakes and creep in the low resistivity zone is consistent with suggestions that seismicity at Parkfield is fluid driven.

INTRODUCTION

The San Andreas fault in California is the boundary between the Pacific and North American plates and is one of the most accessible and well-studied plate margins on Earth (Wallace, 1990). Despite such study, many aspects of its seismicity and structure are still unresolved. In this paper the results of recent high-resolution magnetotelluric (MT) and seismic reflection imaging of the Parkfield segment of this fault are presented. MT is a remote sensing technique capable of imaging subsurface electrical resistivity (Vozoff, 1991). Because fluids dramatically lower the resistivity of their host rocks, the MT method provides a powerful tool for delineating fluids in the crust. The MT data collected at Parkfield strongly suggest that the fault zone beneath Middle Mountain contains anomalously high fluid content. This observation is consistent with recent models of the earthquake cycle by Byerlee (1993) and Rice (1992), in which the presence of high-pressure fluids at depth within faults has been postulated to account for the weakness of strike-slip faults such as the San Andreas (Zoback et al., 1987).

TECTONIC SETTING

Parkfield marks the transition from the creeping central segment of the San Andreas fault to the north to the locked 1857 Fort Tejon earthquake segment to the south. It is the site of six moderate earthquakes within the past 150 years, the most recent being an $M = 5.9$ event in 1966 (Bakun and Lindh, 1985). Owing to the apparent regularity of characteristic earthquakes on this segment of the San Andreas fault, Parkfield has been the focus of a major monitoring effort aimed at a better understanding of the earthquake cycle and possible precursory phenomena (Bakun and Lindh, 1985). Parkfield is also a potential site for a scientific fault-zone drilling project (Hickman et al., 1994). The San Andreas fault at

Parkfield separates very different types of basement rock (Fig. 1; Sims, 1990; Dibblee, 1980). Southwest of the San Andreas fault basement rock is Salinian granite, which is overlain by Quaternary and Tertiary sediments. To the northeast the basement is Franciscan, a melange consisting primarily of metamorphosed accretionary prism, covered by Tertiary and Holocene sediments. Seismic reflection showed that fault-normal compression has produced a flower structure 5 km or more wide in the upper 10 km of the

crust (McBride and Brown, 1986). The absence of coherent reflectors suggests a zone of heavily fractured material in the fault zone. Fault-zone-guided waves that propagate within a wedge of low seismic velocity material along the fault, provide more direct evidence for a fractured zone (Li et al., 1990). Tomographic velocity analysis using microearthquake sources (e.g., Eberhart-Philips and Michael, 1993; Lees and Malin, 1990; Michelini and McEvilly, 1991) reveals lower seismic velocities northeast of the San

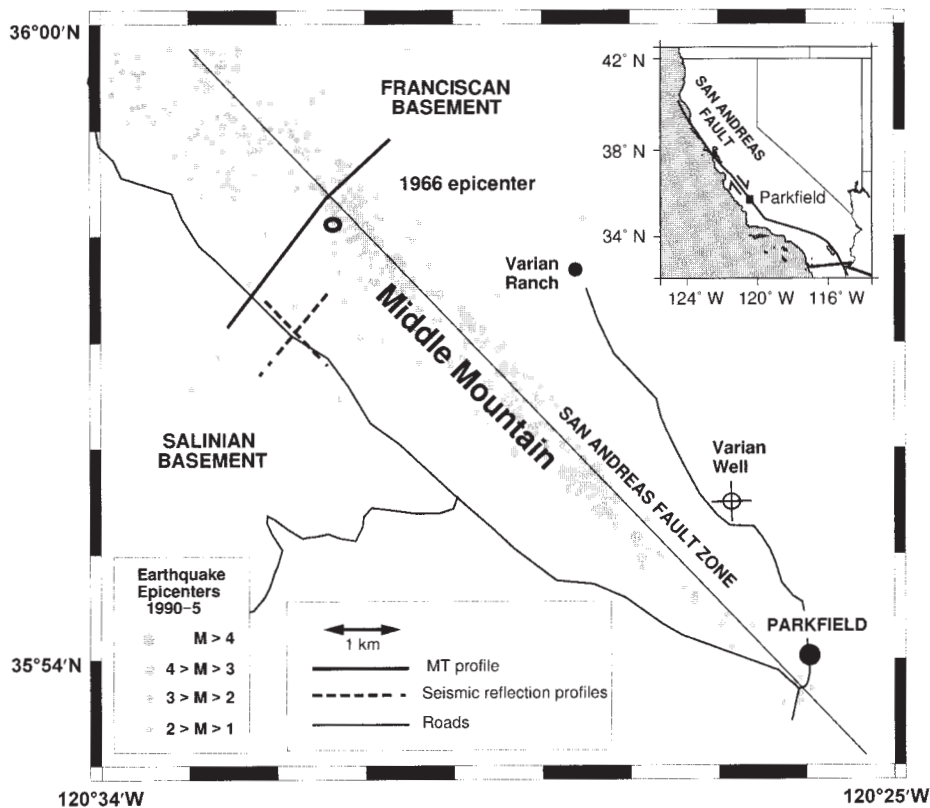


Figure 1. Map of San Andreas fault in vicinity of Parkfield showing location of magnetotelluric (MT) and seismic surveys.

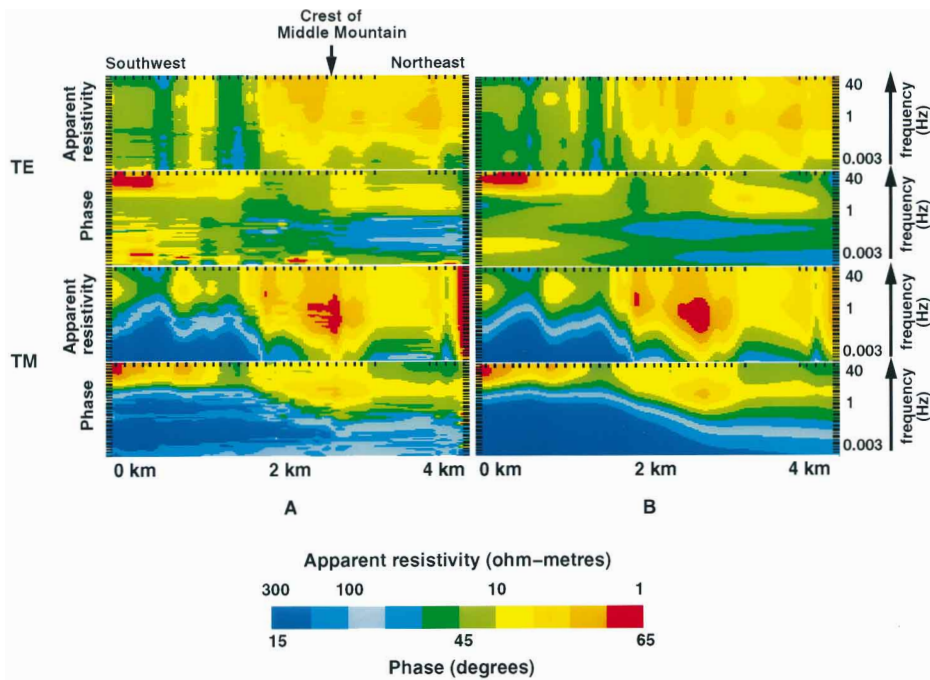


Figure 2. A: Continuous magnetotelluric data collected at Middle Mountain. Ticks on horizontal axis denote locations at which data were recorded. These locations are spaced 100 m apart except for a gap east of Middle Mountain. Vertical axis is frequency. Because low frequencies penetrate farthest into the earth, this form of display gives an impression of depth. Transverse electric (TE) apparent resistivity was computed from currents flowing parallel to fault and magnetic fields normal to fault. Transverse magnetic mode (TM) apparent resistivity was computed from currents flowing across fault and magnetic fields parallel to fault. Phase is proportional to the derivative of the apparent resistivity with respect to frequency. A uniform earth would give a constant phase of 45° and in general high phases correspond to low resistivity and vice versa. **B:** Response of the resistivity model (Fig. 3B) that best fits MT data.

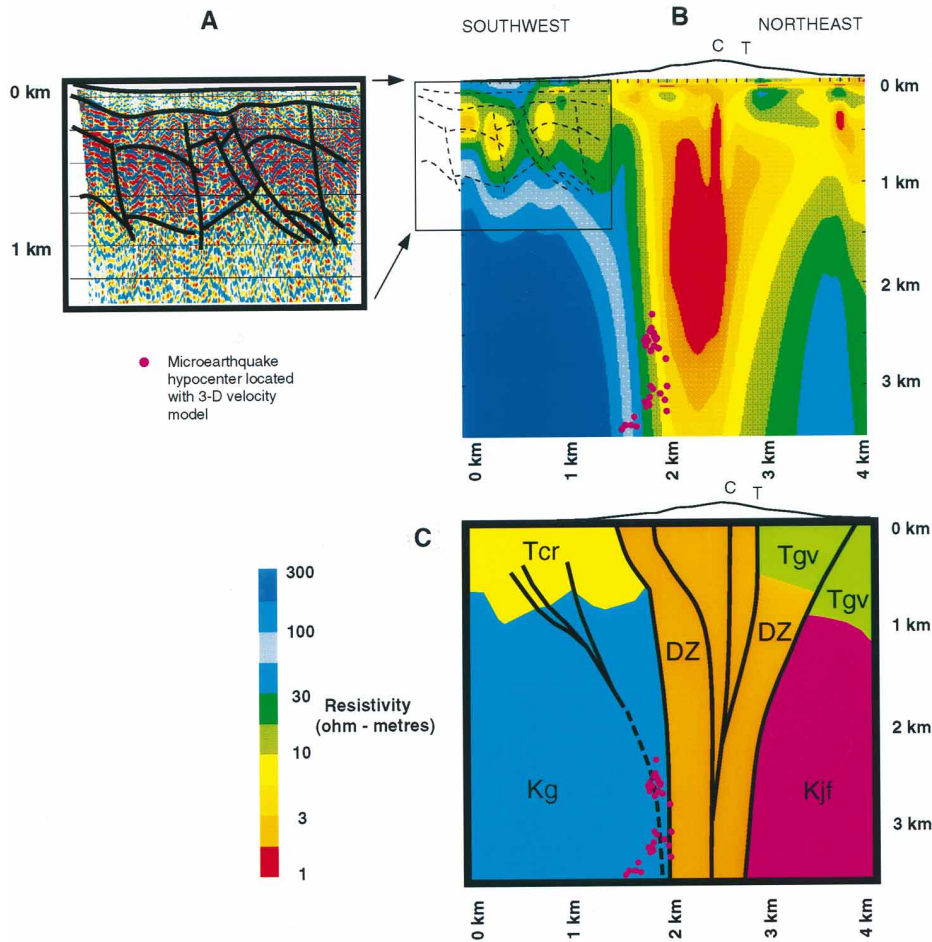


Figure 3. A: Migrated seismic reflection data on profile normal to fault. The depth of 1 km corresponds to a two-way travel time of 1 s. **B:** Electrical resistivity model that best fits observed magnetotelluric data presented in Figure 2. Location of active trace on basis of creep is denoted by T and topography shown on same vertical scale. **C:**—crest of Middle Mountain. **C:** Schematic interpretation of the seismic and magnetotelluric data. Kg—Salinian granite, Tcr—Coast Range sedimentary units, Tgv—Tertiary Great Valley sequence, Kjf—Franciscan melange, and DZ—damaged zone.

Andreas fault. Regional MT measurements suggest that low electrical resistivities are associated with these low velocities, but site spacing was too wide to resolve detailed fault zone structure (Eberhart-Philips and Michael, 1993; Park et al., 1991). Direct current (DC) resistivity measurements by Park and Fitterman (1990) suggest a complicated near-surface resistivity structure in the Parkfield area.

DATA ACQUISITION

The high-resolution MT measurements described here were designed to image the electrical resistivity of the fault zone close to the 1966 epicenter (Fig. 1). Along the 4 km profile, electric fields were measured continuously with 100 m dipoles, and magnetic fields were measured every 500 m. Variations in these fields in the frequency range of 40 Hz to 0.003 Hz were recorded for 6–10 hrs and then analyzed using the technique of Egbert and Booker (1986) to determine the apparent resistivity and phase as a function of surface position and frequency (Fig. 2A). Because low-frequency signals penetrate deeper than high-frequency signals, plotting frequency on the vertical axis gives an impression of how resistivity varies with depth. A number of features can be qualitatively identified in the data sections (Fig. 2A). On the southwest end of the profile, the apparent resistivity computed from electric currents that cross the San Andreas fault (TM mode) reveals a resistive body beneath a shallow conductive layer. Northeast of the fault, resistivities appear to be significantly lower, and the lowest resistivities occur beneath the crest of Middle Mountain.

The tensor decomposition technique of Chave and Smith (1994) demonstrated that electrical resistivity variations along strike are small enough to justify a two-dimensional interpretation. The two-dimensional minimum structure inversion technique of Smith and Booker (1991) was then used to convert the apparent resistivity and phase data into electrical resistivity as a function of

depth (Fig. 3B), and data were fit to within 5% (Fig. 2B). Equal weight was given to vertical and horizontal smoothing. The inversion generates the smoothest resistivity model consistent with the data, and all structures in the resulting model are required by the data. More complex models may also fit the data, but additional structure is not required. Note that the model becomes smoother as depth increases because the deeper parts of the model are sampled by longer wavelength signals than the top.

Multichannel seismic reflection data were collected west of the San Andreas fault (Fig. 1) to locate the top of the Salinian granite. Two 22–88 Hz Vibroseis profiles were shot, one parallel to the San Andreas fault and one normal to it. Each profile consisted of 128 fixed receiver points at 15.2 m intervals. Alternate receiver points were used as source points. The data were then analyzed with a simple common midpoint reflection processing sequence, to permit a simple time-to-depth conversion (Fig. 3A).

GEOLOGIC INTERPRETATION

Southwest of the San Andreas fault the resistivity model and the seismic section independently show a rough surface at a depth of 700–900 m separating rocks of significantly different physical properties. The high electrical resistivity and uniform seismic impedances below this surface indicate that it is the faulted top of the Salinian granites. Above this contact both data sets suggest that the overlying Tertiary sedimentary rocks are faulted and folded. The lateral resistivity variations within these rocks probably result from fault-controlled concentrations of ground water, and it is inferred that the faults may act as flow barriers. Northeast of the San Andreas fault, drilling at the Varian well penetrated 1700 m of briny sedimentary rocks before encountering Franciscan basement in a low-angle fault zone containing pressurized water in large fractures (Jongmans and Malin, 1995). The low resistivities east of the fault, which extend to depths of ≈ 1500 m in the MT model, are consistent with the well data, and suggest a zone of fluid-rich sediments extending several km east of the San Andreas fault.

LOW RESISTIVITY FAULT ZONE

The most striking feature of the resistivity model of Figure 3B is the vertical zone of low electrical resistivity ($< 5 \Omega \cdot \text{m}$) beneath Middle Mountain. Modeling and inversion of the MT data require the resistivity of this zone to significantly increase at ≈ 4000 m. A thinner zone of low resistivity may exist at greater depths, but this is not resolvable from surface MT measurements (Eberhart-Philips et al., 1995).

What is the origin of this low resistivity? Serpentinite, a rock that can have low resistivity, has been found at many locations along the San Andreas fault, but no surface exposures were

mapped on Middle Mountain by Sims (1990), Dibblee (1980), or Dickinson (1966). Aeromagnetic data have been used by Hanna et al. (1972) to locate buried serpentinites along the San Andreas fault, because of the large magnetic anomalies sometimes associated with this material. The absence of such an anomaly at Middle Mountain suggests, but does not require, that a large serpentinite body is absent. Because the aeromagnetic data described by Simpson et al. (1989) were collected on a 1 mile (1.6 km) grid, it is possible that a small serpentinite sliver could have escaped detection. However, serpentinite alone is unlikely to produce the very low resistivities observed ($< 5 \Omega \cdot \text{m}$).

Clay minerals are another candidate for the low resistivity. These minerals are commonly found in fault gouge and may contribute to the weakness of strike-slip faults. Typical clays have resistivities in the range 5–20 $\Omega \cdot \text{m}$ (Palacky, 1987). Although clay may partially explain the low resistivity, the large region with resistivity $\approx 1 \Omega \cdot \text{m}$ suggests another material is responsible for the low resistivity. Within the breccia and fault gouge located in the core of the fault, saline fluids could easily produce a network of interconnected pores and low electrical resistivity. The amount of fluid has been estimated in two ways from the resistivity data.

(1) Fluid is present in interconnected pores. The Varian well a few kilometres along the fault encountered brines with 30 000 ppm chloride. Assuming that these fluids are representative of those in the fault zone, then the fault zone fluids would have a resistivity of $\rho_f = 0.26 \Omega \cdot \text{m}$. Archie's law is often used to convert electrical resistivity to porosity in systems where electrical conduction is dominated by an interconnected pore fluid and is written in the form

$$\rho_r = \rho_f \phi^{-m}$$

where ρ_r is the effective resistivity of the rock, ϕ is the porosity, and m is a constant that lies between 1 and 2. To obtain $\rho_r = 3 \Omega \cdot \text{m}$, typical of the fault zone at 3 km depth, would require a porosity range of 8.6% to 30%, with $m = 1$ and 2, respectively. For the expected texture of a fault zone with cracks, as opposed to spherical pores, the lower $m = 1$ porosity bound is more reasonable. If significant clay content were present, then less fluid would be required to produce the low resistivity.

(2) Fluid is contained in a set of macroscopic cracks. This was the case with the fluids encountered in the Varian well that were located in a narrow fractured zone that is inferred to be one of the eastern strands of the flower structure shown in Figure 3C. Given the resistivity of brine derived above, and assuming a 500-m-wide zone of $3 \Omega \cdot \text{m}$ resistivity anomaly at 3 km, a 30-m-wide zone of fluid would have the same effective conductance (ratio of width and resistivity).

It is most probable that a combination of

macroscopic cracks, interconnected pore fluids, and clay minerals is the cause of the zone of low resistivity. These porosity values are high for near-surface rocks, and although there is some nonuniqueness converting resistivity to porosity, all calculations indicate that a significant fluid content is required to explain the low resistivity.

The low resistivity zone forms a damaged zone at the center of a flower structure. Two branches of the flower structure are inferred to bound the damaged zone. Loci of very low resistivity may indicate faults within the damaged zone. Faults imaged within the sedimentary rocks west of the San Andreas may represent another. The ≈ 500 m horizontal width of the zone of low resistivity agrees well with the width of the seismic low-velocity zone inferred from the fault-zone-guided wave observations of Li et al. (1990). Fracturing and fluid saturation combine to produce low electrical resistivity and seismic velocity. The correlation of these two parameters strengthens the case that the low resistivity is due to fluids, rather than serpentinite or clay alone. The seismic observations also favor a significant width of high porosity because a few narrow cracks alone would not allow guided waves to propagate. Studies of exhumed exposures of the San Gabriel and Punchbowl faults in southern California (Anderson et al., 1983; Chester et al., 1993) showed a wedge of breccia and gouge that pinched out at ≈ 4 km. Both depth extent and shape agree well with the wedge-shaped zone of low resistivity at Parkfield consisting of fluid-saturated breccia.

The fluids could be mantle, crustal, or meteoric in origin. At the Cajon Pass drill site located on the Mojave segment of the San Andreas fault, Torgersen and Clarke (1992) determined that the fluids originated as meteoric water transported at depth within the crust. At Parkfield it is most likely that the inferred fluids are also crustal and enter the fault from the northeast. They could be meteoric in origin or generated by metamorphic reactions in the Franciscan unit (Irwin and Barnes, 1975). Fluid migration may be in response to regional tectonic stresses described by Wentworth and Zoback (1989). This idea is supported by the low electrical resistivity imaged northeast of the San Andreas fault by previous regional MT surveys (Eberhart-Philips and Michael, 1993; Park et al., 1991). Observations of low seismic velocity in this area by Eberhart-Philips and Michael (1993) are also consistent with this pathway for fluid transport. However it is unclear at what depth the fluids enter the fault.

RELATION TO SEISMICITY

Are the fluids related to the seismicity? Numerous microearthquakes, mapped by Nadeau et al. (1995), occur at depths above 4 km on the western edge of the low resistivity zone (Fig. 3). The role of the fluids may be passive, and they may simply come to the surface when they encounter the impermeable granite, using the fault

zone as an easy conduit (Irwin and Barnes, 1975). It is also possible that fluids play a more active role in the earthquake cycle. These fluids could form high-pressure, fluid-filled compartments as suggested by Byerlee (1993). Johnson and McEvilly (1995) suggested that Parkfield seismicity is fluid driven and the MT data support this idea because they show that fluids are present at the depths of at least the shallowest earthquake clusters. It is significant that the earthquakes are located on the edge of the granite block, while the actively creeping surface trace lies to the east of the low resistivity zone (errors in the microearthquake locations are ≈ 200 m). Here the mechanically rigid granite block is strong enough to produce earthquakes. If deformation at depth is also occurring directly beneath the surface trace then it must be accommodated by aseismic creep. Compression of the flower structure causes weak, fluid-saturated material to be uplifted and accounts for the topography of Middle Mountain—a pressure ridge.

The characteristic Parkfield earthquakes occur at depths below those shown in Figure 3. If fluid is flowing up through the fault zone, then high porosities may also exist at depth, implying the characteristic earthquakes may also be fluid driven. Is it coincidental that a high fluid content is observed at the location of the predicted $M = 6$ event? With the available data, we have not determined if the low resistivity is typical of the whole Parkfield segment, or just localized beneath Middle Mountain. That the fluids are electrically conductive may be significant for earthquake prediction. Fraser-Smith and Liu (1995) reported electromagnetic precursors to earthquakes at Parkfield. Motion of a conducting fluid as a high-pressure compartment burst could generate observable electromagnetic precursors to an earthquake.

CONCLUSIONS

The MT data have yielded high-resolution images of the interior of the San Andreas fault zone beneath Middle Mountain. The low resistivity fault core implies clay and saline fluids are present within the cracks of a zone of gouge and breccia that narrows with depth. The high porosities are consistent with the suggestion that seismicity at Parkfield is fluid driven.

ACKNOWLEDGMENTS

This work was supported by U.S. Geological Survey National Earthquake Hazard Reduction Program grant 1434-94-6-2423 and National Science Foundation grant EAR-9316160. The inversion technique was supported by U.S. Department of Energy Grant DE-FG06-92-ER14231. MT fieldwork was made possible by Nong Wu, Xinghua Pu, Weerachai Siripunavaporn, Yuval, Zudman, and support from Electromagnetic Instruments Inc. We thank Kevin Kester and Jack Varian for access to their property; Mark Zoback and Donna Eberhart-Phillips for helpful reviews; and Steve Park, Steve Hickman, and members of the Parkfield working group for discussions.

REFERENCES

- Anderson, J. L., Osborne, R. H., and Palmer, D. F., 1983, Cataclastic rocks of the San Gabriel fault—An expression of deformation at deeper crustal levels in the San Andreas fault: *Tectonophysics*, v. B98, p. 209–251.
- Bakun W. H., and Lindh, A. G., 1985, The Parkfield, California, earthquake prediction experiment: *Science*, v. 229, p. 619–624.
- Byerlee, J., 1993, Model for episodic flow of high pressure water in fault zones before earthquakes: *Geology*, v. 21, p. 303–306.
- Chave, A. D., and Smith, J. T., 1994, Understanding decomposition of magnetotelluric impedance matrices: *Journal of Geophysical Research*, v. 99, p. 4669.
- Chester, F. M., Evans, J. P., and Biegel, R. L., 1993, Internal structure and weakening mechanisms of the San Andreas fault: *Journal of Geophysical Research*, v. 98, p. 771–786.
- Dibblee, T. R., 1980, Geology along the San Andreas fault from Gilroy to Parkfield, in Streitz, R., and Sherburne, R., eds., *Studies of the San Andreas fault zone in northern California*: Sacramento, California Division of Mines and Geology, Special Report 140, p. 3–18.
- Dickinson, W. R., 1966, Structural relationships of the San Andreas fault system and Castle Mountain range, California: *Geological Society of America Bulletin*, v. 77, p. 451–471.
- Eberhart-Phillips, D., and Michael, A. J., 1993, Three-dimensional velocity structure, seismicity and fault structure in the Parkfield region, central California: *Journal of Geophysical Research*, v. 98, p. 15737–15758.
- Eberhart-Phillips, D., Stanley, W. D., Rodriguez, B. D., and Lutter, W. J., 1995, Surface seismic and electrical methods to detect fluids related to faulting: *Journal of Geophysical Research*, v. 100, p. 12919–12936.
- Egbert, G. D., and Booker, J. R., 1986, Robust estimation of geomagnetic transfer functions: *Geophysical Journal of the Royal Astronomical Society*, v. 87, p. 173–194.
- Fraser-Smith, A. C., and Liu, T. T., 1995, ULF magnetic field observations preceding the $M = 5$ earthquake of 20 December 1994 at Parkfield, California: *Eos (Transactions, American Geophysical Union)*, v. 76, p. F360.
- Hanna, W. F., Burch, S. H., Dibblee, T. W., 1972, Gravity, magnetics and geology of the San Andreas fault area near Cholame, California: U.S. Geological Survey Professional Paper 646-C.
- Hickman, S., Zoback, M. D., Younger, L., and Ellsworth, W., 1994, Deep scientific drilling in the San Andreas fault zone: *Eos (Transactions, American Geophysical Union)*, v. 75, p. 137.
- Irwin, W. P., and Barnes, I., 1975, Effect of geologic structure and metamorphic fluids on seismic behavior of the San Andreas Fault system in central and northern California: *Geology*, v. 3, p. 713–716.
- Johnson, P. A., and McEvilly, T. V., 1995, Parkfield seismicity: Fluid driven?: *Journal of Geophysical Research*, v. 100, p. 12937–12950.
- Jongmans, D., and Malin, P. E., 1995, Microearthquake S-wave observations from 0 to 1 km in the Varian well at Parkfield, California: *Bulletin of the Seismological Society of America* v. 85, p. 1805–1821.
- Lees, J. M., and Malin, P. E., 1990, Tomographic images of P-wave velocity variation at Parkfield, California: *Journal of Geophysical Research*, v. 95, p. 21793–21804.
- Li, Y., Leary, P., Aki, K., and Malin, P. E., 1990, Seismic trapped modes in the Oroville and San Andreas fault zones: *Science*, v. 249, p. 763–765.
- McBride, J. H., and Brown, L. D., 1986, Reanalysis of the COCORP deep seismic reflection profile across the San Andreas fault, Parkfield, California: *Bulletin of the Seismological Society of America* v. 76, p. 1668–1686.
- Micheline, A., and McEvilly, T. V., 1991, Seismological studies at Parkfield, I—Simultaneous inversion for velocity structure and hypocenters using cubic b-splines parameterization: *Bulletin of the Seismological Society of America*, v. 81, p. 524–552.
- Nadeau, B., Foxall, W., and McEvilly, T. V., 1995, Clustering and periodic recurrence of microearthquakes on the San Andreas fault at Parkfield, California: *Science*, v. 267, p. 503–507.
- Palacky, G., 1987, Resistivity characteristics of geologic targets, in Naibighian, M. N., ed., *Electromagnetic methods in applied geophysics*: Tulsa, Oklahoma, Society of Exploration Geophysicists, v. 1, p. 53.
- Park, S. K., and Fitterman, D. V., 1990, Sensitivity of the telluric monitoring array in Parkfield, California to changes in resistivity: *Journal of Geophysical Research*, v. 95, p. 15557–15571.
- Park, S. K., Biasi, G. P., Mackie, R. L., and Madden, T. R., 1991, Magnetotelluric evidence for crustal suture zones bounding the Great Valley, California, *Journal of Geophysical Research*, v. 96 p. 353–376.
- Rice, J. R., 1992, Fault stress states, pore pressure distributions, and the weakness of the San Andreas fault, in Evans, B., and Wong, T. F., eds., *Earthquake mechanisms and transport properties of rocks*: London, Academic Press, p. 475–503.
- Simpson, R. W., Jachens, R. C., and Wentworth, C. W., 1989, Average topography, isostatic residual gravity, and aeromagnetic maps of the Parkfield region, California: U.S. Geological Survey Open-File report 89–13.
- Sims, J. D., 1990, Geologic map of the San Andreas fault in the Parkfield, 7.5-minute quadrangle, California: U.S. Geological Survey Miscellaneous Field Studies Map, MF-2115, scale 1:24 000, 1 sheet.
- Smith, J. T., and Booker, J. R., 1991, Rapid inversion of two- and three-dimensional magnetotelluric data: *Journal of Geophysical Research*, v. 96, p. 3905–3922.
- Torgersen, T., and Clarke, W. B., 1992, Geochemical constraints on formation fluid ages, heat flux and crustal mass transport mechanisms at Cajon Pass: *Journal of Geophysical Research*, v. 97, p. 5031–5038.
- Vozoff, K., 1991, The magnetotelluric method, in Naibighian, M. N., ed., *Electromagnetic methods in applied geophysics*: Tulsa, Oklahoma, Society of Exploration Geophysicists, v. 2, p. 641.
- Wallace, R., 1990, The San Andreas fault system, California: U.S. Geological Survey Professional Paper 1515, 283 p.
- Wentworth, C. M., and Zoback, M. D., 1989, The style of late Cenozoic deformation at the eastern front of the California coast ranges: *Tectonics*, v. 8, p. 237–249.
- Zoback, M. D., and twelve others, 1987, New evidence on the state of stress of the San Andreas fault system: *Science*, v. 238, p. 1105–1111.

Manuscript received August 14, 1996
 Revised manuscript received December 16, 1996
 Manuscript accepted January 15, 1997